Magnetic Resonance in Medicine 51:807–815 (2004)

The Effect of Gradient Sampling Schemes on Measures Derived From Diffusion Tensor MRI: A Monte Carlo Study

Derek K. Jones*

There are conflicting opinions in the literature as to whether it is more beneficial to use a large number of gradient sampling orientations in diffusion tensor MRI (DT-MRI) experiments than to use a smaller number of carefully chosen orientations. In this study, Monte Carlo simulations were used to study the effect of using different gradient sampling schemes on estimates of tensor-derived quantities assuming a *b*-value of 1000 smm^{-2}. The study focused in particular on the effect that the number of unique gradient orientations has on uncertainty in estimates of tensor-orientation, and on estimates of the trace and anisotropy of the diffusion tensor. The results challenge the recently proposed notion that a set of six icosahedrally-arranged orientations is optimal for DT-MRI. It is shown that at least 20 unique sampling orientations are necessary for a robust estimation of anisotropy, whereas at least 30 unique sampling orientations are required for a robust estimation of tensor-orientation and mean diffusivity. Finally, the performance of sampling schemes that use low numbers of sampling orientations, but make efficient use of available gradient power, are compared to less efficient schemes with larger numbers of sampling orientations, and the relevant scenarios in which each type of scheme should be used are discussed. Magn Reson Med 51:807–815, 2004. Published 2004 Wiley-Liss, Inc.†

Key words: sampling schemes; electrostatic respulsion; cone of uncertainty; trace; anisotropy; rotational invariance

Diffusion tensor magnetic resonance imaging (DT-MRI) (1,2) permits the noninvasive assessment of water diffusion characteristics in vivo. In DT-MRI, a series of diffusion-weighted (DW) images with diffusion-encoding gradients applied in noncollinear and noncoplanar directions are acquired and the tensor is computed via linear or nonlinear regression (1). Since the symmetric diffusion tensor has six unique elements, one can estimate the tensor from just six DW images acquired with the encoding gradients applied along six unique orientations (plus one non-DW image). However, due to noise, more images are usually acquired, which results in an overdetermined system and allows for more robust tensor estimation. Since only six unique sampling directions are required, however, the value of sampling schemes in which more unique orientations are used is not immediately clear.

This issue was first addressed by Papadakis et al. (3) and later by Skare et al. (4), who studied various DT-MRI sampling schemes in terms of the variance of fractional anisotropy (FA) measurements as a function of tensor orientation. Papadakis et al. (3) demonstrated that a scheme employing 24 unique sampling directions outperformed a scheme with only six directions. Skare et al. (4) concluded that for estimating anisotropy, a scheme with 30 unique sampling directions (5) outperformed a scheme with only six unique sampling directions. Neither study addressed the question, at what number between six and 30 directions is no significant benefit derived from increasing the number of sampling directions further, i.e., when do diminishing returns occur? This issue was later addressed for the specific task of estimating anisotropy (i.e., what is the minimum number of unique sampling orientations required for robust estimation of anisotropy?) (6). Three measures of anisotropy were considered, and simulations were performed assuming a tensor with a fixed anisotropy (λ_1: λ_2: λ_3 = 12:1:1). Papadakis et al. (6) concluded that the minimum number of unique encoding directions, N_e, required for robust anisotropy estimation was $18 \leq N_e \leq 21$.

However, in a later study, Hasan et al. (7) used different criteria to assess sampling-scheme performance, and assumed a tensor with a different anisotropy (λ_1 : λ_2: λ_3 = 4:1:1). They concluded that there is no advantage to using more than six sampling orientations as long as the selected orientations point to the vertices of an icosahedron. Batchelor et al. (8) recently lent support to this notion by suggesting that icosahedral schemes are functionally equivalent to a sampling scheme in which an infinite number of orientations are sampled and are therefore, by definition, rotationally invariant. (However, see Ref. 9 for a brief discussion of why the assumptions used to make this assertion are violated.)

These studies focused mainly on the influence of the sampling scheme on measures of anisotropy. However, the influence of the gradient sampling scheme on estimates of mean diffusivity and tensor orientation remains unknown. Another issue that remains to be addressed concerns the benefit of employing "efficient" gradient sampling schemes. Most DT-MRI sampling schemes with more than six sampling directions employ a maximum encoding gradient amplitude that is not larger than the maximum gradient amplitude obtainable along one of the physical axes (i.e., the *x*-, *y*-, or *z*-axis). We refer to these as "unit-sphere" schemes. However, if a limited number of gradient vectors are employed, their orientations can be chosen such that the resultant amplitude can exceed that obtained along the physical axes. We refer to these schemes as "efficient" because they make efficient use of the gradient power

Section on Tissue Biophysics and Biomimetics, Laboratory of Integrative Medicine and Biophysics, National Institute of Child Health and Human Development, National Institutes of Health, Bethesda, Maryland.

*Correspondence to: Derek K. Jones, National Institutes of Health, Building 13, Room 3W16E, 13 South Drive, Bethesda, MD 20892-5772. E-mail: jonesde@mail.nih.gov

Received 4 September 2003; revised 1 December 2003; accepted 1 December 2003.

DOI 10.1002/mrm.20033
Published online in Wiley InterScience (www.interscience.wiley.com).

available. Here we consider two such schemes: the commonly used dual-gradient scheme (10,11), in which gradients are applied simultaneously along two physical axes at the maximum gradient amplitude, and an efficient version of the icosahedral arrangement initially proposed by Muthupallai et al. (12). In the former, the resultant gradient amplitude is greater than that obtained in the unit-sphere schemes by a factor of $\sqrt{2}$. In the latter, the icosahedral arrangement is rotated with respect to the coordinate system defined by the physical axes of the gradient system, so as to maximize the resultant gradient vector amplitude. The amplitude along one axis is then the maximum gradient amplitude, while the amplitude along the second axis is equal to the maximum gradient amplitude multiplied by Fibonacci's golden ratio (13), $f_r = (\sqrt{5} - 1)/2$. In a study using numerical optimization, this scheme was recently shown to provide the most optimal arrangement of six gradients for DT-MRI in terms of minimizing the orientational variation in estimates of anisotropy (7).

The advantage of the efficient gradient schemes is that a given effective diffusion weighting can be achieved with shorter-duration gradients compared to those used for unit-sphere schemes. This allows a shorter echo time (TE) to be obtained and reduces the transverse (T_2) relaxation, and thus yields an enhanced signal-to-noise ratio (SNR) per unit time. The Appendix shows how an approximation to the gain in SNR (relative to the unit-sphere schemes) can be computed for both schemes.

The conflicting data in the literature and the unanswered questions prompted us to investigate further the effect of gradient sampling scheme direction on the results obtained from DT-MRI experiments.

MATERIALS AND METHODS

Gradient Encoding Schemes

Since one aim of this study was to investigate the effect of varying the number of *unique* gradient sampling directions, a total number of DW images was sought that had a reasonable number of closely spaced integer factors, f_n (where $f_n \geq 6$). To this end, we settled on a total of 60 DW images (f_n = 6, 10, 12, 15, 20, 30, and 60). For each unique number of sampling vectors, the orientations were defined by the electrostatic repulsion algorithm previously proposed by Jones et al. (5). The n unique sampling vectors are likened to a series of n "rods" with a point charge at each end. The rod orientations are iteratively modified so as to maximize the sum of the squared distances between all possible "pairs" of charges, effectively minimizing the sum of the electrostatic repulsive forces. This produces encoding schemes with almost rotationally invariant condition numbers (4,8), and, for appropriate numbers of gradient orientations, the arrangements correspond to the vertices of Platonic solids. For example, for six directions, the electrostatic repulsion scheme produces vectors that point to the vertices of an isosahedron (P. Batchelor, personal communication). Papadakis et al. (6) later described a modification to this algorithm in which the repulsive forces between charges were modeled following an r^{-n} law (where n is progressively made > 2).

To test the benefits of using the efficient schemes, we compared the performances of the dual-gradient scheme originally proposed by Davis et al. (10) (i.e., [$+xy$, $+xz$, $+yz$, $-xy$, $-xz$, $-yz$]) and the efficient icosahedral scheme proposed by Muthupallai et al. (12) to that of a scheme in which 30 directions were distributed uniformly using the electrostatic algorithm. The SNRs for the three schemes were appropriately modified (see Appendix) such that the ratio of the SNRs for the three schemes (i.e., 30 directions : efficient dual gradient : efficient icosahedral) was 1: 1.328: 1.151.

Tensor Simulations

To simulate biologically relevant characteristics, diffusion tensors, **D**, were simulated with constant Trace ($Tr(\mathbf{D}) = 2.1 \times 10^{-3}$ mm^{2}s^{-1}) (11) but varying FA (14) and orientation. First, a diagonalized tensor was simulated with eigenvalues (λ_1, λ_2 and λ_3) given by

$$\lambda_1 = (\mathrm{Tr}(\mathbf{D})/3)(1 + 2FA/(3 - 2FA^2)^{1/2})$$

$$\lambda_2 = \lambda_3 = (\mathrm{Tr}(\mathbf{D})/3)(1 - FA/(3 - 2FA^2)^{1/2}). \quad [1]$$

Tensors with different orientations, **D′**, were then obtained via the similarity transform:

$$\mathbf{D}' = \mathbf{R}^{\mathrm{T}}\mathbf{D}\mathbf{R},$$

where **R** is the rotation matrix. For each value of FA, 500 different orientations of the tensor (uniformly spaced over the hemisphere) were simulated.

Noise Simulation

Sixty-one images (one image with no diffusion gradients applied, and 60 DW images) were simulated for each experiment. The combinations of encoding directions (number of unique directions/number of repeats of each direction for each experiment) were as follows: (6/10), (10/6), (12/5), (15/4), (20/3), (30/2), and (60/1).

For each scheme, the noise-free DW intensity, I, was determined for each sampling direction according to:

$$I = I_0 \exp(-\mathrm{Trace}(\mathbf{bD})), \quad [3]$$

where I_0 is the unweighted signal, and, for a given sampling direction $|g_x, g_y, g_z|$,

$$\mathbf{b} = b\begin{bmatrix} g_x^2 & g_xg_y & g_xg_z \\ g_xg_y & g_y^2 & g_yg_z \\ g_xg_z & g_yg_z & g_z^2 \end{bmatrix}, \quad [4]$$

where the resultant diffusion weighting of b = 1000 s/mm^2 was assumed for each encoding direction.

Different levels of Gaussian random noise were then added in quadrature to both the noise-free DW signals and the noise-free unweighted signal, to give SNRs in the b = 0 image of 5, 10, 15, 20, and 25. The (noisy) tensor was then recomputed from the noise-contaminated DW sig-

nals. This was repeated a total of N_{MC} times (where N_{MC} = 10000) for each orientation of the diffusion tensor.

Characterizing Rotational Variance

For each noisy estimate of **D**, the trace, FA, and principal eigenvector were determined, giving a distribution of N_{MC} values at each orientation. For the trace and FA, the mean of the N_{MC} estimates was computed for each orientation. To characterize the distribution in the eigenvector estimates at each noise-free orientation, the 95% cone of uncertainty (CU) was computed as described elsewhere (15). Briefly, the mean eigenvector was determined by finding the mean of 10000 dyadic tensors, where each dyadic tensor is formed by taking the outer product of the principal eigenvector with itself, i.e.:

$$\langle \boldsymbol{\epsilon}_1^j \boldsymbol{\epsilon}_1^{j^T} \rangle = \left\langle \begin{pmatrix} (\varepsilon_{1x}^j)^2 & \varepsilon_{1x}^j \varepsilon_{1y}^j & \varepsilon_{1x}^j \varepsilon_{1z}^j \\ \varepsilon_{1x}^j \varepsilon_{1y}^j & (\varepsilon_{1y}^j)^2 & \varepsilon_{1y}^j \varepsilon_{1z}^j \\ \varepsilon_{1x}^j \varepsilon_{1z}^j & \varepsilon_{1y}^j \varepsilon_{1z}^j & (\varepsilon_{1z}^j)^2 \end{pmatrix} \right\rangle = \frac{1}{N_{MC}} \sum_{j=1}^{N_{MC}} \boldsymbol{\epsilon}_1^j \boldsymbol{\epsilon}_1^{j^T}. \quad [5]$$

The principal eigenvector $\bar{\Psi}_1$ of the mean dyad, $\langle \boldsymbol{\epsilon}_1^j \boldsymbol{\epsilon}_1^{j^T} \rangle$ and the angular deviation between each of the 10000 Monte Carlo estimates of $\boldsymbol{\epsilon}_1^j$ and the mean orientation $\bar{\Psi}_1$ were determined by:

$$\theta^j = \cos^{-1}(\bar{\Psi}_1 \cdot \boldsymbol{\epsilon}_1^j). \quad [6]$$

A histogram of the N_{MC} values of θ^j was constructed, and the 95th percentile was taken as the 95% confidence angle or CU.

For each quantity (trace, *FA*, and CU) two summary measures were determined: 1) the mean taken over the 500 orientations; and 2) the standard deviation (SD) taken over the 500 orientations (4).

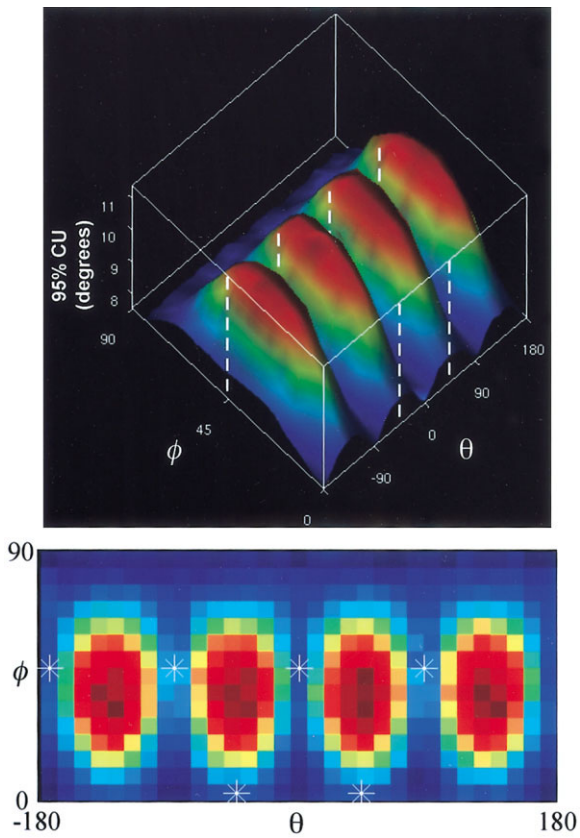

FIG. 1. Variation in the 95% CU in degrees, as function of tensor orientation (FA = 0.9, SNR = 15), for the dual-gradient sampling scheme (10,11). The azimuth and elevation angles are represented by θ and ϕ, respectively. In the upper panel, the variation is represented as a 3D surface (which we term the "response surface") and the orientations of the sampling vectors are represented as dotted white lines. In the lower panel, the surface has been collapsed onto a 2D plane and white stars represent the position of the sampling vectors.

RESULTS

Figure 1 shows the 95% CU as a function of tensor orientation for the dual-gradient sampling scheme (10,11). This scheme yields large variations in orientational uncertainty as a function of tensor orientation, with variations of approximately 50% over the range of orientations.

Figure 2 illustrates the CU as a (θ, ϕ) response surface for six different sampling schemes in which the number of unique sampling directions varies between six and 60, and the total number of DW images is the same (i.e., 61). There is a marked reduction in the mean CU and an increased "flatness" of the surface when the number of unique sampling orientations increases from six to 10. Further improvements (albeit less marked) are seen when the number of sampling orientations is further increased.

Figure 3 shows how the mean (i.e., the mean of the 500 estimates) and SD of the CU varies with the number of sampling orientations for two different SNRs and a range of FAs. The reduction in the mean CU with an increasing number of unique orientations is most marked for tensors with higher anisotropy. For example, in Fig. 3a, for tensors with FA = 0.9, the mean CU is reduced by approximately 4° by moving from six unique sampling orientations to 10, while there is minimal change in the mean CU observed for tensors with lower anisotropy (e.g., FA = 0.4). The benefit of increasing the number of sampling orientations becomes more pronounced as the SNR decreases.

The advantage of increasing the number of unique orientations, in terms of reducing the SD, becomes more pronounced as the anisotropy increases–but for all levels of anisotropy, an asymptotic behavior is observed. Following Papadakis et al. (6), we assessed the value of N_e for which increasing the number of sampling directions further had a minimal effect by looking at the differential change of the SD with respect to N_e. The value of N_e for which the differential change oscillated about zero was deemed to be the point of "diminishing returns." In this case, the limit was reached at 30 unique sampling directions.

Figure 4 shows the variation in estimated FA over the 500 orientations—both as a surface (Fig. 4a) for a particular anisotropy (FA = 0.9) and as a plot (Fig. 4b) for a range of anisotropies. In this case, the asymptotic number of sampling directions is approximately 20.

Figure 5 shows the SD of the measurements of the trace of the diffusion tensor obtained over the 500 orientations

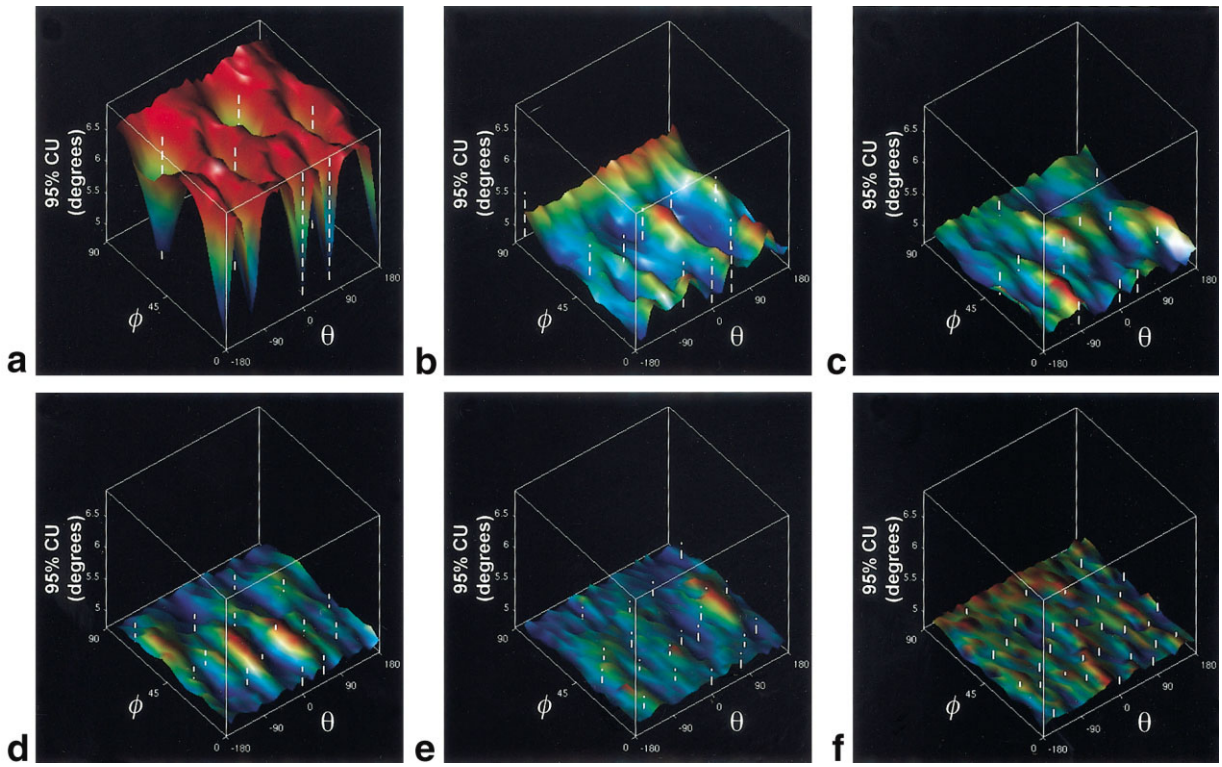

FIG. 2. Variation in the 95% CU in degrees, as function of tensor orientation for tensors with FA = 0.9 and SNR = 15, for six different sampling schemes. For all panels (**a–f**), the total number of DW images simulated is the same (61), but the number of unique sampling orientations (arranged using the electrostatic repulsion algorithm of Jones et al. (5)), varies. The number of unique sampling orientations is (**a**) 6, (**b**) 10, (**c**) 12, (**d**) 15, (**e**) 20, and (**f**) 30.

(SNR = 15). Again, the advantage of increasing N_e is clearly demonstrated, with the effect becoming more pronounced as FA increases. Here the limit for diminishing returns (as defined above) is reached at 30 unique directions, similar to the results obtained for the 95% CU in Fig. 3.

We compared the 95% CU as a function of orientation obtained with the unit-sphere gradient scheme (Fig. 6a), utilizing 30 unique sampling orientations (5) (termed the "Jones30" scheme by Skare et al. (4)), with the results obtained using the efficient dual-gradient scheme (Fig. 6b) and the efficient icosahedral scheme (both of which utilize six unique sampling orientations). Clearly, the Jones30 scheme produces the flattest response of the three schemes. The dotted white line shows the mean of the measurements obtained using this scheme (6.96°). Unsurprisingly, improving the efficiency of the other two schemes (i.e., allowing the resultant gradient vectors to fall beyond the unit sphere) does not affect the topology of the response surface much, but it does lower the overall uncertainty. With the efficient dual-gradient scheme (Fig. 6b), the majority of the estimates of the CU fall below the average value obtained with the Jones30 scheme (67.1% of the CU estimates are $< 6.96°$). However, there are four broad peaks in the surface corresponding to tensor orientations in which the uncertainty in ϵ_1 is substantially larger than the average Jones30 value. In contrast, with the efficient icosahedral scheme (Fig. 6c), most of the CU estimates are larger than that obtained with the Jones30 scheme (albeit with a few sharp "valleys" in the response

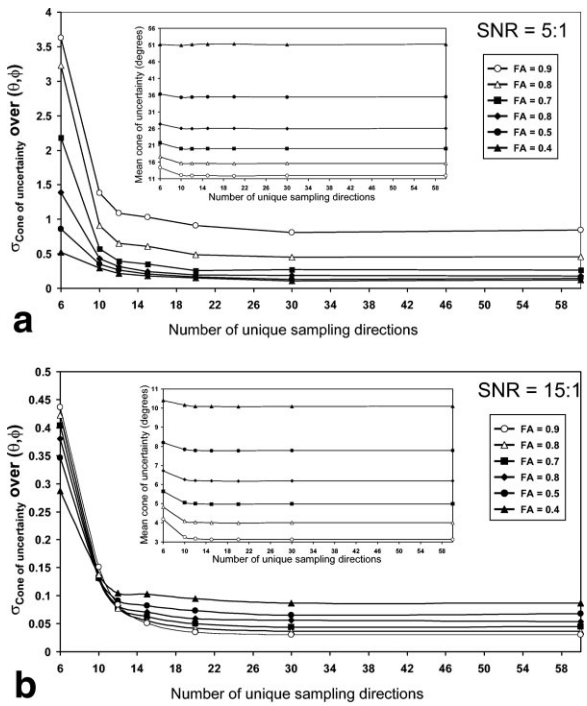

FIG. 3. Dependence of the mean (inset) and SD in the 95% CU (i.e., the mean and SD of the values obtained over the 500 orientations) on the number of unique sampling orientations, for simulated tensors with FA ranging from 0.4 to 0.9. The figure shows results obtained at two different SNRs: (**a**) 5:1 and (**b**) 15:1.

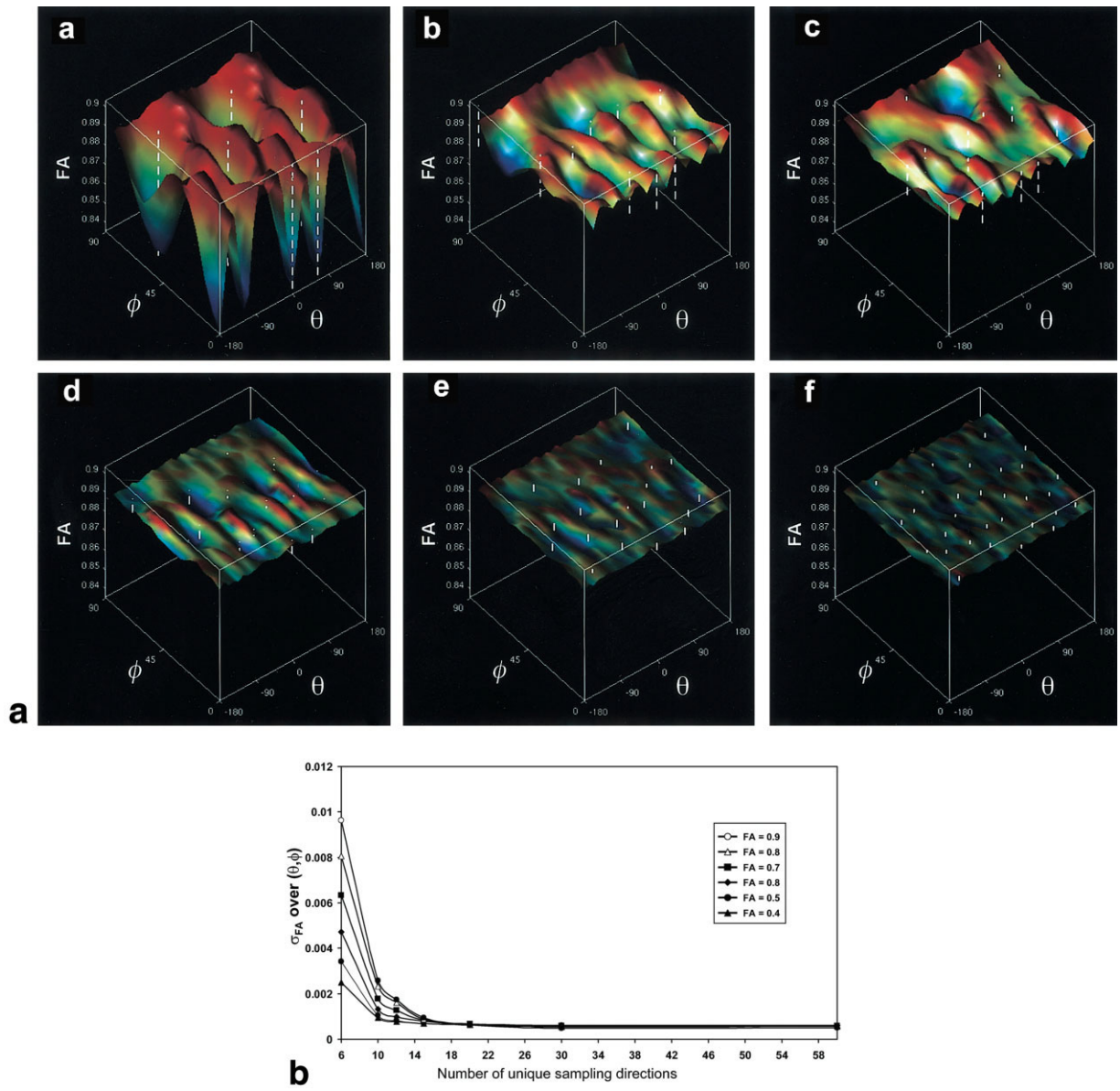

FIG. 4. **a:** Variation in the estimated FA as a function of tensor orientation for tensors with FA = 0.9 and SNR = 15:1, for six different sampling schemes. For each scheme, the number of unique sampling orientations is (**a**) 6, (**b**) 10, (**c**) 12, (**d**) 15, (**e**) 20, and (**f**) 30. **b:** Dependence of the variance in FA measurements (variance of the measurements obtained at 500 different orientations) on the number of unique sampling orientations for simulated tensors with a range of anisotropies.

surface, in which the uncertainty is less than the average). For this scheme, 85.8% of the CU estimates are above 6.96°.

DISCUSSION

By examining Figs. 1 and 2, the reader can get an intuitive feel for the benefit of using sampling orientations that are both numerous and uniformly spaced. One can think of the response surface as a rubber sheet, and the sampling vectors as "fingers" that push down on the sheet. When the fingers push down, the response surface tends to bulge between the sampling vectors. The more fingers used, the flatter the surface response. Using the same analogy, one can envisage the result of different spacings of a fixed number of sampling vectors. The maxima and minima of the response surfaces in Figs. 1 and 2a also indicate the benefit of uniformly arranging the sampling vectors.

Figure 3 indicates that in terms of the absolute uncertainty in the tensor orientation, there is a clear advantage in moving from six to 10 unique sampling directions, but little advantage thereafter. Again, the effect is most marked for low SNR and high anisotropy.

In terms of the SD in the CU, the benefit of increasing the number of sampling directions further is also demonstrated in Fig. 3. The SD of the CU over the range of 500 orientations (a surrogate marker of the "flatness" of the surface response) decreases as the number of sampling directions is increased. Again, this effect is more pronounced at lower SNR and for tensors with higher anisot-

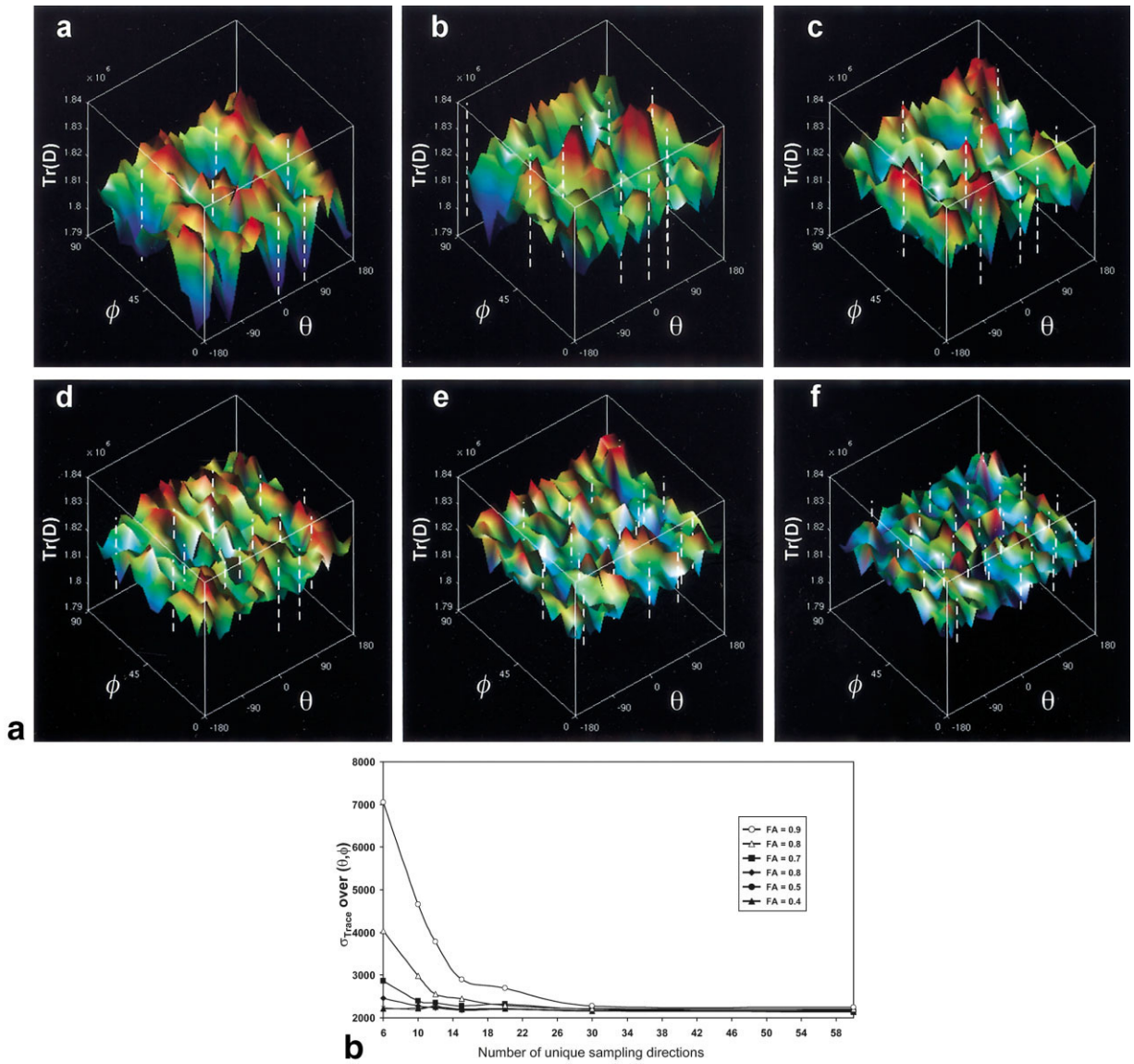

FIG. 5. a: Variation in the estimated trace of the diffusion tensor as function of tensor orientation for tensors with FA = 0.9 and SNR = 15, for six different sampling schemes. The number of unique sampling orientations in each scheme is (**a**), 6, (**b**) 10, (**c**) 12, (**d**) 15, (**e**) 20, and (**f**) 30. **b:** Dependence of the variance in trace measurements (variance of the measurements obtained at 500 different orientations) on the number of unique sampling orientations for simulated tensors with a range of anisotropies.

ropy, but the point at which increasing the number of unique sampling orientations further had a minimal effect, considering a range of SNRs and anisotropies, was approximately 30.

Figure 4 shows the variation in FA with tensor orientation as a function of the number of unique sampling orientations. The topology of the response surface in Fig. 4a is very similar to that seen in Fig. 2. This is perhaps unsurprising given the relationship between uncertainty in orientation and FA reported elsewhere (15). It is interesting that the point at which increasing the number of unique sampling orientations further has a minimal effect (i.e., the differential change oscillates about zero) occurred at approximately 20 unique sampling orientations. This is in perfect accord with the findings of Papadakis et al. (6).

Figure 5 shows a previously unreported effect: the dependence of estimates of mean diffusivity (classically a "rotationally invariant" quantity (11)) on the sampling orientation. As stated previously, the effect depends on the anisotropy, but for high anisotropy (FA $\geq$ 0.7), the asymptotic value of number of unique encoding directions is approximately 30.

Not unexpectedly, Fig. 6 shows that improving the efficiency of a particular sampling scheme by simply rotating the fixed set of gradient vectors with respect to the axes defined by the physical axes of the gradients, but *without* changing the orientation of the gradient vectors with respect to each other, has little effect on the *topology* of the response surface.

Implications for Experimental Design

The trace is fairly uniform in parenchyma at *b*-values typically used clinically ($b \leq 1000$ s/mm^2) (11). This

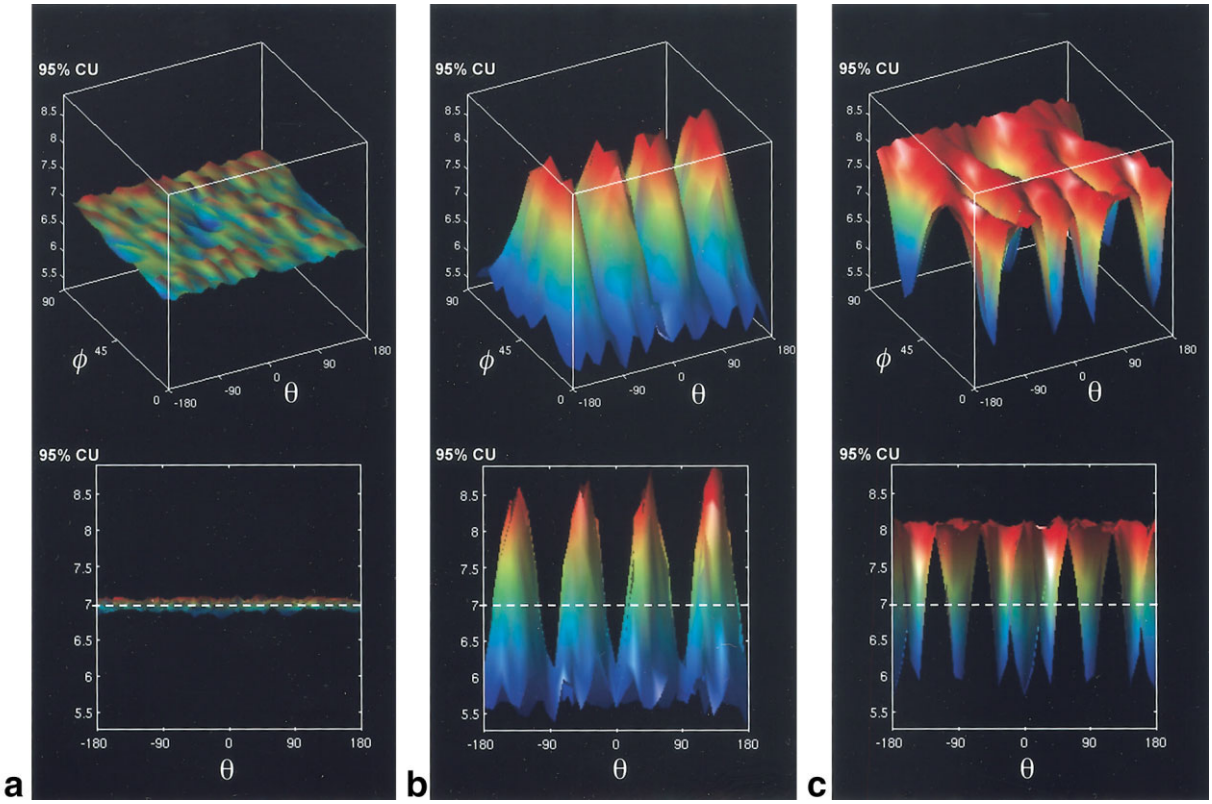

FIG. 6. Comparison of the performance of three sampling schemes: (**a**) Jones30 (30 unique directions), (**b**) efficient dual-gradient (six unique directions repeated five times), and (**c**) efficient icosahedral (six unique directions repeated five times), in terms of the variation in the 95% CU as a function of tensor orientation for a tensor with FA = 0.90 and SNR = 15:1. Two views of the surface are shown for each result to allow the topology to be fully appreciated. The dotted horizontal white line in the lower panel shows the mean of the 500 estimates of the CU obtained with the Jones30 scheme. In the response obtained with the dual-gradient scheme (**b**), the majority of values fall below this average, but there are four wide peaks where the CU is substantially larger than this average. With the efficient icosahedral scheme, the majority of values are substantially larger than the average value obtained with the Jones30 scheme, with a few sharp valleys.

study shows that sampling schemes with fewer than 30 unique directions introduces variations in estimates of mean diffusivity that are solely attributable to the different orientation of the tissue. These variations will effectively increase the SD of measurements obtained from a region of interest encompassing voxels containing tissue with different fiber orientations. Such increased variance will reduce statistical power for intrasubject comparisons of mean diffusivity in different regions of the brain, and will in general spuriously increase the heterogeneity of the apparent trace within the parenchyma. One can consider the implications of this artifactual heterogeneity for studies that use histogram analyses to compare data from subjects. Using a scheme with more unique sampling orientations, rather than fewer, will reduce the width of the histograms and may increase the conspicuity of *real* patient-control differences. The same arguments apply to analyses of regions of uniform diffusion anisotropy.

Of course, in a clinical situation in which it is necessary to scan patients as quickly as possible, it may be impractical to acquire 30 DW images for each slice location. Nevertheless, this study has shown that if time is available for collecting more than the bare minimum of DW images (i.e., six DW images and one non-DW image), then *unique* sampling orientations should be chosen, rather than repeats of the same set of sampling orientations. In other words, one should collect DW data in as many unique (and uniformly spaced) sampling orientations as time will allow.

One can consider the importance of a carefully designed sampling scheme for diffusion tensor tractography (16–25) by conducting a simple thought experiment. Consider two perfectly straight fiber bundles with uniform and high anisotropy. One bundle is aligned with the *x*-axis, and the other is aligned with the *y*-axis. We have shown that without due care, the DT-MRI sampling scheme can introduce a bias such that the CU depends on fiber orientation. Consequently, one could consider a scheme in which the uncertainty in fiber orientation is much greater for fibers aligned with the *x*-axis than for those aligned with the *y*-axis. With such a scheme, the "connectivity," is assessed in terms of the number of trajectories passing along the tract, would appear to be greater along the *y*-axis than along the *x*-axis; hence, the sampling scheme would have introduced bias into our connectivity estimates.

An interesting question is, if only the bare minimum of DW images are to be collected (i.e., six DW images and one non-DW image), then which sampling scheme should be

used? As noted earlier, Hasan et al. (7), using numerical optimization, determined that the most optimal arrangement of six sampling vectors, in terms of minimizing the "total variance" (i.e., the variance of estimates of tensor elements as a function of tensor orientation), was the efficient icosahedral scheme (which was also used in the present study). They also showed that the efficient dual-gradient scheme was suboptimal and represented a local maximum in their optimization process.

Are there any benefits, then, to using the efficient dual-gradient scheme? Clearly, of the three schemes examined here (Jones30, efficient dual-gradient, and efficient icosahedral), the efficient dual-gradient scheme permits the shortest TE for a given diffusion weighting, and hence yields an improved SNR per unit time (see Appendix). The sensitivity of anisotropy measures to noise is now a well-documented phenomenon (28), with estimates of the anisotropy of tissue being increasingly positively biased as the SNR decreases. Consequently, in the low-SNR domain, estimates of anisotropy will be less biased with the efficient dual-gradient scheme than with any other scheme. We have shown in this study that the use of such schemes introduces substantial orientational bias in tensor-derived quantities. However, depending on the application, this form of bias may be of less concern than maximizing the SNR per unit time. For example, in a serial study of diffusion characteristics in a particular lesion (e.g., a multiple sclerosis lesion), the patient will be oriented in approximately the same manner for each successive scan session. Consequently, the orientational bias introduced by a scheme like the efficient dual-gradient scheme will be of little concern, and one may choose to focus on obtaining measures of anisotropy that are the least affected by the noise-induced bias reported by Pierpaoli et al. (28). Further, if one is only interested in characterizing diffusion within gray matter (in which diffusion is isotropic at the voxel length scale), then no orientational bias will be presented, and, again, the efficient dual-gradient scheme should be employed.

Without doubt, the most useful application of diffusion imaging to date is in the study of acute ischemia (29,30), where the prime interest is looking for reductions in the trace of the diffusion tensor. As the reduction is typically of the order of 30%, the variation in trace values due to differences in orientation seen in Fig. 5a are again going to be of little concern. In that particular application, it would be preferable to maximize the SNR and hence use a sampling scheme that places the sampling vector amplitudes beyond the unit sphere, such as the efficient dual-gradient or efficient icosahedral schemes described above.

Our results were obtained exclusively from Monte Carlo simulations, and have not been validated in vivo. However, a validation of these findings would necessitate orienting an anisotropic structure (such as a white-matter fasciculus) in 500 different orientations within the scanner, which would clearly be impossible. It would be possible to perform such a validation using an anisotropic diffusion phantom that could be more readily reoriented within the scanner. However, to date, such a phantom has not been designed.

CONCLUSIONS

Our results show that robust determination of mean diffusivity, FA, and tensor orientation requires a DT-MRI sampling scheme in which at least 30 unique and evenly distributed sampling orientations are employed. (The optimal arrangement of 30 sampling orientations obtained by use of the electrostatic repulsion algorithm (as employed in this study) was previously tabulated in Ref. 4.) However, for anisotropy measurements only, the measurements will be robust when at least 20 unique sampling orientations are used. Schemes with a lower number of sampling orientations can introduce biases and correlations between tensor orientation and apparent diffusion characteristics, even if they make efficient use of available gradient strength. For applications such as fiber-tractography, and particularly "probabilistic" approaches, one should use as many unique sampling orientations as time will allow. However, when time is limited and only the minimum number of DW images can be collected for DT-MRI (i.e., six DW images and one non-DW image), in most cases the efficient dual-gradient scheme should be employed. In summary, when designing a DT-MRI experiment, one should consider 1) the type of information to be extracted from the diffusion tensor, and what biases may be introduced by the sampling scheme; and 2) the amount of imaging time available. The choice of sampling scheme will then become a trade-off between minimizing bias and minimizing scan time.

ACKNOWLEDGMENTS

I thank Dr. Peter Basser and Dr. Carlo Pierpaoli for helpful discussions and encouraging comments during the course of this work, and Liz Salak for reviewing the manuscript.

APPENDIX

In this Appendix, we aim to estimate the improvement in SNR per unit time of the efficient sampling schemes as compared to the unit-gradient schemes. It is assumed that the DT-MRI acquisition is based on a conventional DW spin-echo sequence and that the duration of the imaging gradients is minimal, such that the duration of the diffusion encoding gradients, δ, is equal to TE/2.

Using the standard Stejskal-Tanner expression (26) for the diffusion weighting, b,

$$b = \gamma^2 G^2 \delta^2 \left(\Delta - \frac{\delta}{3} \right), \qquad [A1]$$

where G is the amplitude of the diffusion-encoding gradients, Δ is their temporal separation, and γ is the gyromagnetic ratio, and assuming that $\delta = \Delta = TE/2$, an approximate expression for TE is obtained:

$$TE \approx \left(\frac{12b}{\gamma^2 G^2} \right)^{1/3}. \qquad [A2]$$

If we now define the ratio of the maximum gradient amplitudes applied in an efficient scheme to that applied in

the unit-gradient scheme as α, then from Eq. [A2] the ratio of TEs using the two schemes is found to be

$$\frac{TE_{\text{efficient}}}{TE_{\text{unit sphere}}} = (\alpha)^{-(2/3)}. \quad [A3]$$

We can then define the ratio of the SNRs, κ, as

$$\kappa = \frac{SNR_{\text{efficient}}}{SNR_{\text{unit sphere}}} = \exp\left(\frac{TE_{\text{unit sphere}} - TE_{\text{efficient}}}{T_2}\right) = \exp\left(\frac{TE_{\text{unit sphere}}(1 - \alpha^{-(2/3)})}{T_2}\right). \quad [A4]$$

For the efficient dual-gradient scheme (10,11), $\alpha = 1.414$, whereas for the efficient icosahedral scheme (12), $\alpha = 1.176$. Assuming a typical TE for a unit-sphere gradient sampling scheme of 110 ms and a white-matter T_2 of 80 ms (27), $\kappa = 1.328$ for the dual gradient scheme, and $\kappa = 1.151$ for the efficient icosahedral sampling scheme.

REFERENCES

1. Basser PJ, Matiello J, Le Bihan D. Estimation of the effective self-diffusion tensor from the NMR spin echo. J Magn Reson B 1994;103: 247–254.
2. Basser PJ, Matiello J, Le Bihan D. MR diffusion tensor spectroscopy and imaging. Biophys J 1994;66:259–267.
3. Papadakis NG, Xing D, Houston GC, Smith JM, Smith MI, James MF, Parson AA, Huang CL-H, Hall LD, Carpenter TA. A study of rotationally invariant and symmetric indices of diffusion anisotropy. Magn Reson Imaging 1999;17:881–892.
4. Skare S, Hedehus M, Moseley ME, Li TQ. Condition number as a measure of noise performance of diffusion tensor data acquisition schemes with MRI. J Magn Reson 2000;147:340–352.
5. Jones DK, Horsfield MA, Simmons A. Optimal strategies for measuring diffusion in anisotropic systems by magnetic resonance imaging. Magn Reson Med 1999;42:515–525.
6. Papadakis NG, Murrills CD, Hall LD, Huang CL-H, Carpenter TA. Minimal gradient encoding for robust estimation of diffusion anisotropy. Magn Reson Imaging 2000;18:671–679.
7. Hasan KM, Parker DL, Alexander AL. Comparison of gradient encoding schemes for diffusion-tensor MRI. J Magn Reson Imaging 2001;13:769–780.
8. Batchelor P. Optimisation of direction schemes for diffusion tensor imaging. In: Proceedings of the Workshop on Diffusion MRI: Biophysical Issues (What Can We Measure?), St Malo, France, 2002.
9. Jones DK. When is DT-MRI sampling scheme *truly* isotropic? In: Proceedings of the 11th Annual Meeting of ISMRM, Toronta, Canada, 2003. p 2118.
10. Davis TL, Wedeen VJ, Weisskoff, Rosen BR. White matter tract visualization by echo-planar MRI. In: Proceedings of the 12th Annual Meeting of SMRM, New York, 1993. p 289.
11. Pierpaoli C, Jezzard P, Basser PJ, Barnett AS. Diffusion tensor MR imaging of the human brain. Radiology 1996;201:637–648.
12. Muthupallai R, Holder CA, Song AW, Dixon WT. Navigator aided, multishot EPI diffusion images of brain with complete orientation and anisotropy information. In: Proceedings of the 7th Annual Meeting of ISMRM, Philadelphia, 1999. p 1825.
13. Dunlap RA. The golden ratio and Fibonacci numbers. Singapore: World Scientific; 1997. p 1–30.
14. Basser PJ, Pierpaoli C. Microstructural and physiological features of tissue elucidated by quantitative-diffusion-tensor MRI. J Magn Reson B 1996;111:209–219.
15. Jones DK. Determining and visualizing uncertainty in estimates of fiber orientation from diffusion tensor MRI. Magn Reson Med 2003;49:7–12.
16. Mori S, Crain BJ, Chacko VP, van Zijl PC. Three dimensional tracking of axonal projections in the brain by magnetic resonance imaging. Ann Neurol 1999;45:265–269.
17. Conturo TE, Lori NF, Cull TS, Akbudak E, Snyder AZ, Shimony JS, McKinstry RC, Burton M, Raichle ME. Tracking neuronal fiber pathways in the living human brain. Proc Natl Acad Sci USA 1999;96: 10422–10427.
18. Jones DK, Simmons A, Williams SCR, Horsfield MA. Non-invasive assessment of axonal fiber connectivity in the human brain via diffusion tensor MRI. Magn Reson Med 1999;42:37–41.
19. Poupon C, Clark CA, Frouin V, Regis J, Bloch I, Le Bihan D, Mangin J. Regularization of diffusion-based direction maps for the tracking of brain white matter fasciculi. NeuroImage 2000;12:184–195.
20. Parker GJM. Tracing fiber tracts using fast marching. In: Proceedings of the 8th Annual Meeting of ISMRM, Denver, 2000. p 85.
21. Tuch DS, Belliveau JW, Wedeen VJ. A path integral approach to white matter tracotgraphy. In: Proceedings of the 8th Annual Meeting of ISMRM, Denver, 2000. p 791.
22. Basser PJ, Pajevic S, Pierpaoli C, Duda J, Aldroubi A. In vivo tractography using DT-MRI data. Magn Reson Med 2000;44:625–632.
23. Koch M, Glauche V, Finsterbusch J, Nolte U, Frahm J, Buchel C. Estimation of anatomical connectivity from diffusion tensor data. NeuroImage 2001;13:S176.
24. Parker GJM, Barker GJ, Buckley DL. A probabilistic index of connectivity (PICo) determined using a Monte Carlo approach to streamlines. In: Proceedings of the ISMRM Workshop on Diffusion MRI: Biophysical Issues, St Malo, France, 2002.
25. Behrens TEJ, Johansen-Berg H, Woolrich MW, Smith SM, Wheeler-Kingshott CAM, Boulby PA, Barker GJ, Sillery EL, Sheehan K, Ciccarelli O, Thompson AJ, Brady JM, Matthews PM. Non-invasive mapping of connections between human thalamus and cortex using diffusion imaging. Nat Neurosci 2003;6:750–757.
26. Stejskal EO, Tanner JE. Spin diffusion measurements: spin echoes in the presence of a time-dependent field gradient. J Phys Chem 1965;42: 288–292.
27. Whittall KP, MacKay AL, Graeb DA, Nugent RA, Li DKB, Paty DW. In vivo measurement of T_2 distributions and water contents in normal human brain. Magn Reson Med 1997;27:34–43.
28. Pierpaoli C, Baser PJ. Toward a quantitative assessment of diffusion anisotropy. Magn Reson Med 1996;36:893–906.
29. Moseley ME, Cohen Y, Mintorovitch J, Chileuitt L, Shimizu H, Kucharczyk J, Wendland MF, Weinstein PR. 1990. Early detection of regional brain ischemia in cats: comparison of diffusion- and T_2-weighted MRI and spectroscopy. Magn Reson Med 1990;14:330–346.
30. Warach S, Chien D, Li W, Ronthal M, Edelman RR. Fast magnetic-resonance diffusion-weighted imaging of acute human stroke. Neurology 1992;42:1717–1723.